# Are alkali activated slag concretes suitable for reinforced concrete in chloride environments?

Muhammed Basheer[a], Qianmin Ma[b], Sreejith Nanukuttan[c], John Provis[d], Kai Yang[a]

a. School of Civil Engineering, University of Leeds, Leeds, UK
b. Faculty of Civil Engineering and Mechanics, Kunming University of Science and Technology, Kunming, China
c. School of Natural and Built Environment, Queen's University Belfast, Belfast, UK
d. Department of Materials Science and Engineering, University of Sheffield, Sheffield, UK

**Abstract:** Alkali-activated slag (AAS) is a clinker-free binder with dense calcium silicate hydrate structure, but poor overall pore structure of the paste system. Due to its high alumina content, it has the potential for high chloride binding capacity. A review of literature since 1980's has indicated that in some cases the chloride diffusion in AAS concrete is lower than the Portland cement (PC) counterparts and is comparable to concretes containing high volumes of supplementary cementitious materials, but this has not been found in all cases. Further, less is known about the effect of mix proportions, including binder content, water-binder ratio, both the type and duration of curing, role of activator, etc. on the rate of transport of chloride ions into AAS concretes. In addition, there is conflicting information on the ability of AAS concretes to delay both the onset and the rate of corrosion of embedded steel reinforcement. This paper presents findings from a number of experimental investigations into AAS concretes, especially focusing on the permeation properties and the corrosion behaviour, with an aim to answer whether AAS concretes are suitable where reinforced concrete structures are exposed to chloride environments.

**Keywords:** AAS, corrosion, permeation properties, pore solution, mix proportions

## 1. Introduction

An alternative to Portland cement (PC) is highly desirable to reduce the high carbon footprint of concrete. One promising approach is to use alkali-activated slag (AAS), which offers the possibility of achieving significant reductions in greenhouse emissions, while achieving mechanical properties comparable to those of PC [1-3].

To become established as a successful alternative to PC-based concrete, AAS must give similar durability and long-term resistance levels to aggressive agents. As such, numerous researches have been carried out to examine the durability performance of AAS. Currently, most relevant studies focus on determining pore structure, transport properties such as gas, water and chloride permeability parameters [4-6], while relatively few information about the corrosion of reinforcing steel in AAS is reported [3, 7]. This trend is unusual, because corrosion is the main cause of premature degradation of reinforced concrete structures.

It is recognized that the passivity of reinforcing steel in concrete, whether based on PC or AAS, is attributed to the formation of a thin passive film on the steel surface [3]. This film is maintained by the high pH of the surrounding concrete, unless the film is damaged by the presence of chloride ions or by a pH drop due to carbonation of the concrete [1, 3, 7]. That is, both transport properties and pore solution characteristics will affect the corrosion behaviour of steel in AAS. Given the differences in raw materials and later hydration process between AAS and PC, the initiation and propagation of corrosion are expected to be different [6].

Against this background, a programme of investigation was developed with the objectives of studying: (i) the chloride transport in various AAS concretes; (ii) the physical and chemical characteristics of the pore structure and the pore solution; (iii) corrosion of embedded steel when these concretes were exposed to an intermittent chloride ponding environment.

## 2. Experimental programme

### 2.1 Raw materials

Ground granulated blast-furnace slag (GGBS) confirming to BS EN 15167-1:2006 [8] was used to manufacture all the

AAS concretes. The GGBS was supplied by Civil and Marine Ltd., UK. Class 42.5 N PC (CEM-I) conforming to BS EN 197-1: 2000 [9]. Sodium silicate solution (WG) with $Na_2O$ % of 12.45 and $SiO_2$ % of 43.60 was used as the activator for GGBS. Industrial grade sodium hydroxide powder with a purity of 99 % was used to adjust the Ms to the required values. A barium based retarder 'YP-1' [10] was used in the AAS concretes to control the setting time. The retarder was dry-blended with GGBS before mixing. A polycarboxylic polymer based superplasticizer with a water content of 40 % was used in the PC concrete mix that was taken into account whilst determining the mixing water content. Crushed basalt from Northern Ireland with size fractions of 20 mm and 10 mm combined in a ratio of 1:1 was used as the coarse aggregate. Natural sand with fineness modulus of 2.53 was used as the fine aggregate.

**2.2 Mix proportions**

Table 1 summarises the mix proportions of concrete examined in this study. Twelve AAS concretes mixes with $Na_2O$ % of 4, 6, and 8 and Ms of WG of 0.75, 1.00, 1.50 and 2.00 were investigated in this research. For the purpose of comparison, one PC concrete mix was manufactured with the total binder content as that of the AAS concretes. The W/B ratio of the AAS concretes was 0.47, not the same as that used for the PC mix. This was essential to ensure that the AAS concretes met the slump requirement. A reduction of W/B ratio to 0.42 for AAS concretes to match with that of PC concrete was found to result in harsh mixes which are not workable.

Table 1 Concrete mix proportion

| Mix NO ($Na_2O$-MS) | $Na_2O$ (%) | Ms | Binder ($Kg/m^3$) | Sodium silicate ($Kg/m^3$) | NaOH ($Kg/m^3$) | Retarder ($Kg/m^3$) | Fine aggregate ($Kg/m^3$) | Coarse aggregate ($Kg/m^3$) |
|---|---|---|---|---|---|---|---|---|
| 4%-0.75 | 4 | 0.75 | 371 | 34.6 | 13.6 | 1.11 | 654 | 1163 |
| 4%-1.00 | 4 | 1.00 | 368 | 45.8 | 11.6 | 1.10 | 655 | 1164 |
| 4%-1.50 | 4 | 1.50 | 362 | 67.7 | 7.8 | 1.08 | 656 | 1167 |
| 4%-2.00 | 4 | 2.00 | 357 | 88.9 | 4.2 | 1.07 | 658 | 1170 |
| 6%-0.75 | 6 | 0.75 | 358 | 19.7 | 19.7 | 1.07 | 654 | 1163 |
| 6%-1.00 | 6 | 1.00 | 354 | 16.8 | 16.8 | 1.08 | 655 | 1165 |
| 6%-1.50 | 6 | 1.50 | 346 | 11.2 | 11.2 | 1.06 | 658 | 1169 |
| 6%-2.00 | 6 | 2.00 | 339 | 5.9 | 5.9 | 1.04 | 660 | 1173 |
| 8%-0.75 | 8 | 0.75 | 346 | 25.4 | 25.4 | 1.02 | 654 | 1163 |
| 8%-1.00 | 8 | 1.00 | 341 | 21.6 | 21.6 | 1.04 | 656 | 1166 |
| 8%-1.50 | 8 | 1.50 | 332 | 14.3 | 14.3 | 1.02 | 658 | 1171 |
| 8%-2.00 | 8 | 2.00 | 322 | 7.5 | 7.5 | 0.97 | 661 | 1175 |
| PC | - | - | - | - | - | | 686 | 1220 |

Note: superplasticiser of 0.5 % by mass of cement was used for PC mix.

**2.3 Preparation of samples**

Six 250*250*110 mm blocks (three with embedded steel bars while the other three had no steel) along with nine 100 $mm^3$ cubes and Figure 1 shows the concrete blocks with embedded steel bars. Also shown in this figure are the stainless steel bars (hereafter referred to as electrodes) used for measuring the electrical resistivity of the concretes during the cycling ponding/drying regime. The top bar served as the anode and the three bottom bars together acted as the cathode for electrochemical corrosion measurements. Before embedding the steel bars, they were cleaned first with a wire brush and then with a dry cleaning cloth to remove any rust and debris, at which stage they were weighed.

Both the blocks and the cubes were cast by following the procedure given in BS 1881-125:1986 [11]. After casting concrete into moulds, specimens were covered with thin polythene sheets to minimise evaporation of water from the surface of concrete. Approximately 1 h after the concrete surface became stiff, the moulds were covered with a layer of previously wetted hessian and then covered with a layer of polythene sheet. The samples were stored within moulds for 3 days and then, the specimens were demoulded, wrapped in wet hessian and plastic bags, and stored in a constant temperature room at 20 ± 1 $^oC$ for 91 days. The hessian was checked for the moisture condition

at every 2 weeks and rewetted if needed.

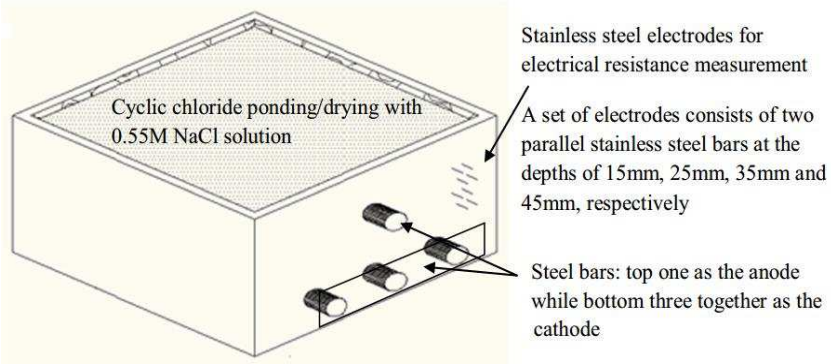


Figure 1 Schematic representation of the concrete block for the corrosion tests

**2.4 Test procedures**

2.4.1 Slump and compressive strength

The slump test specified in BS EN 12350-2:2009 [12] was carried out on the fresh concretes and the compressive strength test according to BS EN 12390-3:2009 [13] was carried out on the 100 mm cubes at 3, 28 and 91 days of age.

2.4.2 Chloride diffusivity

In order to understand chloride transport in the AAS concretes similar to the real exposure environment, non-steady state chloride diffusion test in accordance with NT BUILD 443 [14] was carried out. One day before the test age of 91 days, three cores of diameter 100 mm per mix were cored from the 250*250*110 mm concrete blocks. A slice with a thickness of 50 mm from the casting surface (trowel finished face) was cut off, the rest was kept for carrying out the test. The vacuum saturation regime similar to that of NT BUILD 492 [15] was used to precondition the cores. Before the non-steady state chloride diffusion test, the bulk electrical resistivity of the cores was determined by using a method described in the Chlortest report [16], which is considered to indicate the pore structure of the concrete.

2.4.3 Corrosion of the embedded steel bars

One month before the test age of 91 days, the three concrete blocks with the embedded steel bars (see Fig. 1) were moved to a controlled environment (temperature: 23± 3 ºC, RH: 55±10 %) for 2 weeks. The epoxy resin was applied onto four side surfaces. The blocks were then stored at the above condition for another 2 weeks. Approximately 200 ml of NaCl solution with the concentration of 0.55 M was used to pond the blocks for 1 day followed by 6 days for drying. This cycle of intermittent chloride intermittent ponding was continued until the end of the test (250+ days). During the whole conditioning and testing periods, the blocks were supported by two timber strips to allow air flow under the blocks. At the end of the test, the blocks were split, the anodic steel bars were taken out, scrubbed with wire brush, wiped with a dry cloth and weighed to determine the mass loss caused by the corrosion. The corrosion rate (mm/year) of the steel bars was calculated using the following equation:

$$\text{cossion rate} = \frac{1000 \times m}{A \times t \times \rho} \qquad \text{Eq (1)}$$

where m is the mass loss in gram, q is the density of steel of 7.87 g/cm$^3$, A is the complete surface area of the steel attacked by corrosion in mm$^2$ and t is the test duration in year.

2.4.4 Pore solution expression and bulk electrical resistivity

At the age of 90 days, cores with diameter of 60 mm were cut from the 250*250*110 mm concrete blocks containing no steel bars. A slice with a thickness of 10 mm from the casting surface was cut off. The pre-saturation procedure described in Sect. 2.4.2 was carried out on the cores. The pore solution within the cores was extracted by using a

specialist pore fluid expression device when the cores were subjected to pressures up to 300 tonnes. After collecting the solution, pH and conductivity of the solution were measured immediately by using a pH meter and a conductivity meter. The concentration of $Na^+$ and $S^{2-}$ in the solution was analysed subsequently by using an inductively coupled plasma-optical emission mass spectrometer (ICP-MS) technique.

## 3. Results and discussion

### 3.1 Slump and compressive strength

Table 2 summarises the results of slump and compressive strength of AAS and PC concrete. The slump values show that all the mixes had the slump values with a range from 55 to 180 mms depending on mix proportions. It is clear that the slump values of the AAS concretes increased with the increase of $Na_2O$ %. This is in agreement with the results reported by Allahverdi et al. [17] and Karahan and Yakupoglu [18], which also report the plasticising effect of $Na_2O$ component. The Ms had no significant influence on the slump of the AAS concretes until $Na_2O$ % was increased to 6 %, beyond which the slump increased with the increase of Ms. With the increase of Ms, the increase of $SiO_2$ component in WG increases the viscosity of WG, while total liquid content in AAS concrete (WG + NaOH + additional water) also increases. When more $Na_2O$ was applied, with the increase of Ms, the increase rate of total liquid content was significantly higher than that of $SiO_2$ component, consequently leading to the increase of the slump of the AAS concretes.

Table 2 Slump and compressive strength of the AAS and PC concretes

| Mix NO ($Na_2O$-MS) | Slump (mm) | Compressive strength (MPa) | | |
|---|---|---|---|---|
| | | 3d | 28d | 91d |
| 4%-0.75 | 55 | 22.3±0.1 | 44.7±0.2 | 46.4±1.0 |
| 4%-1.00 | 55 | 21.8±0.1 | 46.7±1.0 | 55.6±0.6 |
| 4%-1.50 | 55 | 1.7±0.0 | 49.5±0.2 | 52.6±2.3 |
| 4%-2.00 | 55 | 1.4±0.0 | 33.3±0.4 | 44.1±0.1 |
| 6%-0.75 | 65 | 31.7±0.7 | 47.3±0.0 | 51.8±2.4 |
| 6%-1.00 | 65 | 37.3±0.2 | 53.6±0.0 | 59.1±0.8 |
| 6%-1.50 | 65 | 20.3±0.7 | 60.8±0.1 | 67.4±2.6 |
| 6%-2.00 | 75 | 8.0±0.0 | 59.6±0.2 | 68.7±2.1 |
| 8%-0.75 | 70 | 32.3±0.0 | 51.9±0.1 | 56.2±0.2 |
| 8%-1.00 | 105 | 32.7±2.4 | 53.6±0.1 | 67.1±0.6 |
| 8%-1.50 | 145 | 34.1±0.7 | 59.3±3.2 | 70.5±2.5 |
| 8%-2.00 | 180 | 11.7±0.2 | 55.4±0.2 | 65.0±0.8 |
| PC | 50 | 35.4±1.2 | 58.9±1.8 | 66.3±2.3 |

The compressive strength of the concretes at the ages of 3, 28 and 91 days are reported in Table 2. The presence of the retarder had affected compressive strength development in AAS concretes, particularly at the early age. The increase of $Na_2O$ % generally increased the compressive strength of the AAS concretes, which is in agreement with the results reported by the others due to increasing amount of C-S-H [1,2]. The AAS concretes with Ms of 1.50 generally obtained the highest compressive strength, which agrees with the results reported previously [19]. It is noted that the PC reference mix has a similar compressive strength with AAS mixes with 6% $Na_2O$, but the W/B ratio of AAS concretes is 0.47, higher than that of the PC concrete (0.42).

### 3.2 Chloride diffusivity, electrical response and pore solution

The non-steady state chloride diffusion coefficient ($D_{nssd}$) of the AAS concretes is compared with that of the PC concrete in Fig. 2. It can be seen that the $D_{nssd}$ of the former was much lower than of the PC reference despite a higher W/B ratio. This suggests that the AAS concretes offer better resistance to chloride ingress. As indicated in Fig.2, the $D_{nssd}$ of the AAS concretes decreased with the increase of $Na_2O$ % from 4 to 8. Al-Otaibi [20] and Karahan and Yakupoglu [18] have reported that porosity of AAS decreases with an increase of $Na_2O$ %. Meanwhile, the

hydration degree of GGBS increases with the increase of $Na_2O$ % [2]. More hydration products would be formed in the AAS with a higher $Na_2O$ % that increases the binding capacity of either/both chlorides and/or their accompanying sodium cations. Both factors have contributed to the explanation of the effect of $Na_2O$ % on $D_{nssd}$. It is also found that Ms around 1.50 is optimum for the hydration of AAS using which gives the reduced porosity and enhanced binding capacity of AAS, naturally leading to the lowest $D_{nssd}$.

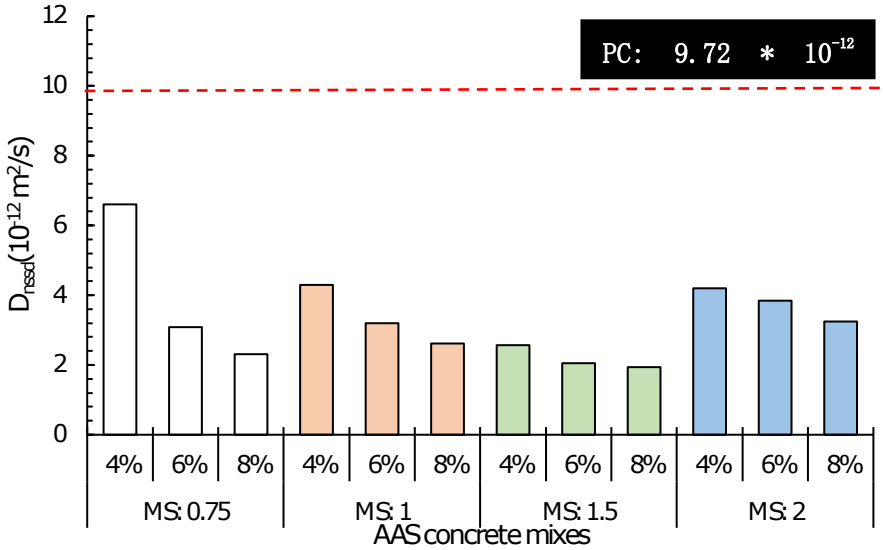


Figure 2 Non-steady state chloride diffusion coefficients of the concretes

The bulk electrical resistivity of the concretes was measured in an attempt to indicate the pore structure of the concretes and to further explain the $D_{nssd}$ results. Figure 3-a shows the results of bulk resistivity of AAS. It is clear that the resistivity of AAS concretes is much high than the PC. It is known that electrical resistivity is significantly affected by the pore solution conductivity of the concrete and the bulk resistivity alone cannot be used to represent the pore structure of concretes [21]. As such, the pore solution conductivity of the concretes was also measured and its reciprocal (pore solution resistivity) was plotted in Fig. 3-b. This figure shows that the AAS concretes have lower pore solution resistivity than the PC concrete. According to the model proposed by Whittington et al. [22], the reason for the higher bulk resistivity of the AAS concretes could be attributed to their tortuous pore structure and/or their lower conductive binder matrix. When the pore solution is highly ionic and conductive (i.e. poorly resistive), the conductivity of binder matrix will be insignificant. In Fig. 2, despite the AAS concretes being less resistive compared to the PC counterpart (as per Fig. 3), they exhibited lower chloride diffusivity. This can happen only if the pore structure is very dense and tortuous [5]. That is, it can be inferred that the relative better chloride diffusivity of AAS concrete is the result of their improved microstructure of the solid phases.

C-S-H (type I), C-A-S-H and hydrotalcite are the main hydration products in AAS [40] and they have much potential to bind alkali cations [1,2]. Substantial amount of $Na^+$ had been introduced into the AAS concretes at the beginning of the mixing. However, after 3 months of curing, a dramatic reduction in the concentration of free $Na^+$ was observed in the AAS concretes, as reported in Table 3. This would suggest that during the transport of chlorides, there is a potential for significant binding of the accompanying sodium cations by the hydrates to occur in the AAS concretes. Secondly, it is clear that the pH value in AAS is much lower than PC and outward diffusions of alkali materials from the concrete into the chloride source solution during the test could be a main reason for the pH reduction, where $OH^-$ is considered to be the main contributor [2]. When such outward diffusion occurs in PC concrete, $Ca(OH)_2$ would dissolve in the pore solution to buffer its alkalinity [1]. However, $Ca(OH)_2$ is not one of the hydration products of AAS. Without the buffering effect, the loss of alkalinity would be more severe in the case of

the AAS concretes. The lower pH for the AAS concretes (refer to Table 3) could also have enhanced their chloride binding capacity due to a competition in absorption between $Cl^-$ and $OH^-$ [23], which also could reduce the $D_{nssd}$.

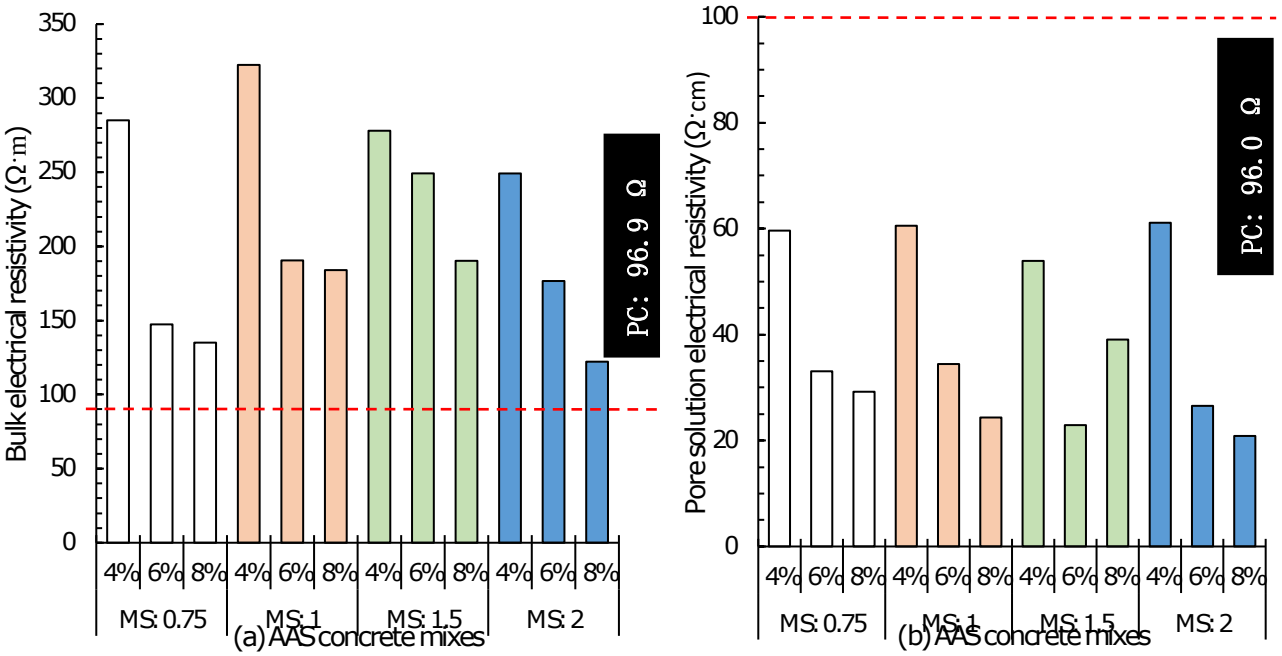


Figure 3 Bulk and pore solution electrical resistivity of AASC and PC concretes

Table 3 pH, $Na^+$ and $S^{2-}$ of the pore solution of AAS concrete after 3 month of curing

| Mix NO ($Na_2O$-MS) | pH | $Na^+$ (ppm) | $S^{2-}$ (ppm) |
|---|---|---|---|
| 4%-0.75 | 11.7 | 2154 | 2458 |
| 4%-1.00 | 11.9 | 4740 | 1953 |
| 4%-1.50 | 10.5 | 58.96 | 3786 |
| 4%-2.00 | 9.9 | 121.2 | 4348 |
| 6%-0.75 | 11.9 | 96.26 | 5661 |
| 6%-1.00 | 11.9 | 69.19 | 6210 |
| 6%-1.50 | 11.4 | 42.18 | 6245 |
| 6%-2.00 | 919 | 18.20 | 6292 |
| 8%-0.75 | 12.4 | 202.0 | 664.0 |
| 8%-1.00 | 12.2 | 244.0 | 590.0 |
| 8%-1.50 | 10.8 | 185.3 | 618.3 |
| 8%-2.00 | 11.9 | 64.34 | 608.0 |
| PC | 12.5 | 1234 | 329.6 |

### 3.3 Corrosion of the embedded steel

Figure 4 shows the corrosion rates of steel bar in AAS and PC concrete specimens. As shown in Fig. 4, the corrosion rate of the steel bars in the AAS concretes depends on the mix proportions and some mixes did give a fast corrosion rate in comparison to that of the PC concrete. Figure 4-b compares corroded steel bars in AAS and PC concrete specimens. It can be seen that the steel bar in the AAS concretes was corroded significantly with most of the steel surface area covered in corrosion products along with occasional pits. This is not an expected observation, because the AAS concretes in this study have better pore structure and lower chloride diffusivity, which should give a low corrosion rate of the embedded steel bars. The reason for the trivial improvement in performance of the steel bars in the AAS concretes could be attributed to the outward diffusion of ions from the concrete cover into the exposure solution during the intermittent chloride ponding. Outward diffusion of alkali materials may have resulted in the reduction of the pH values in the concrete cover (see Table 3). Without the buffering of $Ca(OH)_2$ in the AAS concretes, the continuous diffusion could have resulted in the dissolution of the binder from the cover concrete. Furthermore,

carbonation may have occurred during the drying period, which could also have resulted in the disintegration of the binder of the concrete cover. This is particularly important for AAS concrete [20].

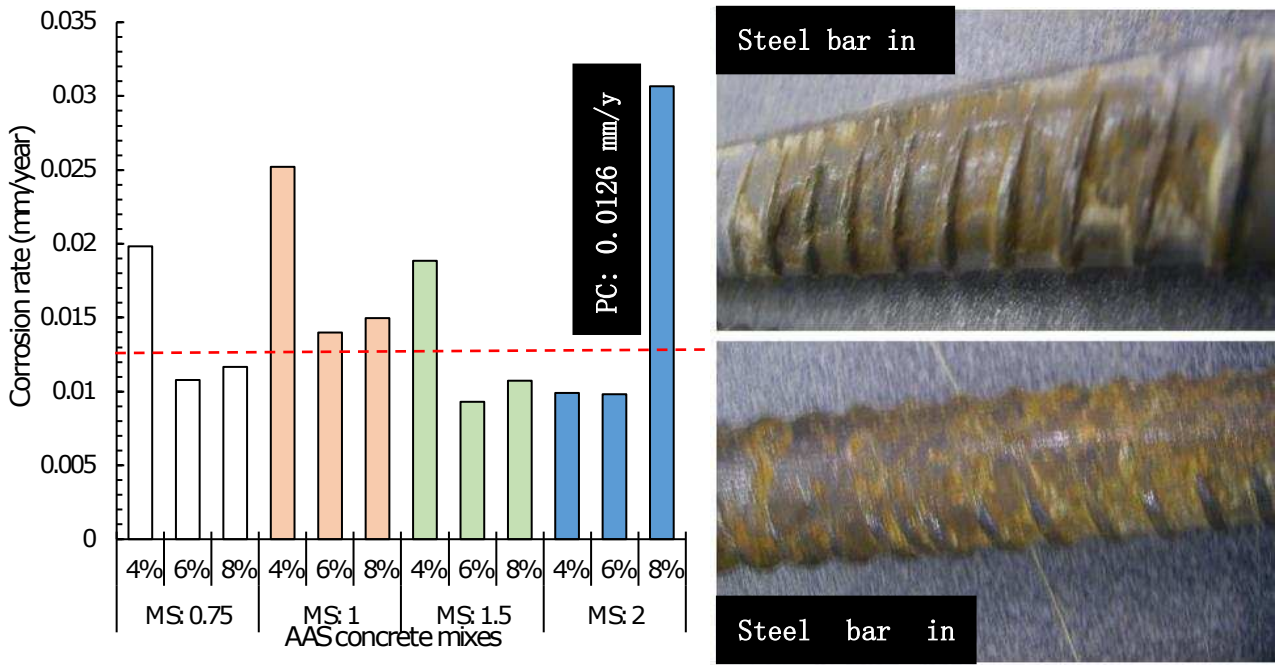


(a) Corrosion rate (b) Corrosion of the anodic steel bar

Figure 4 Corrosion rates calculated from the gravimetric mass loss of steel and corrosion of anodic steel bars at the end of the exposure regime

Figure 5 plots corrosion rates against different influencing factors. In Fig. 5-a and -b, it seems that both chloride diffusivity and bulk resistivity cannot strongly affect corrosion rate of steel in AAS. The possible reasons for the lack of any correlation are as follows: (i) in addition to chloride diffusivity and bulk resistivity, corrosion rate of the embedded steel in concrete is also dependent on the availability of oxygen and water, and concentration of sulphides in the pore solution of the concrete; (ii) absorption occurs in the chloride intermittent ponding regime which is not the case for the immersion test and consequently the chloride transport in these two cases will be different. The disintegration of the binder at the surface of the AAS concretes may also have contributed to such a difference. From Fig. 5-c and –d, it can be seen that there is a fairly good correlation between the corrosion rate of steel and the concentration of sulphides ($S^{2-}$) and $Na^{+}$ in the pore solution for the concretes studied. As expected [3], the corrosion rate generally decreased with the increase of the concentration of sulphides. Presence of sulphides in pore solution of concrete can significantly reduce the redox potential of the pore solution. Redox potential measurement is a reflection of oxidation and reduction activities. The reduction of the redox potential is a result of the increase of reduction atmosphere, which would protect the embedded steel from its oxidation to a certain extent to reduce the corrosion rate of the steel. The concentration of $Na^{+}$ also strongly affects the corrosion rate, more $Na^{+}$, faster corrosion. This can be explained due to losing the $Cl^{-}$ binding capacity in the system, as discussed in previous section.

**4. Conclusion**

On the basis of results obtained, the following conclusions can be drawn:

1) Compared to the PC concrete, the AAS concretes could achieve lower non-steady state diffusion coefficient, if the mix proportion is optimised, as a significant influence and interaction between both $Na_2O$ % and Ms of

water glass can be identified.

2) The corrosion rate of the steel bars in the AAS concretes was comparable to that observed in the PC concrete under the intermittent chloride ponding regime. However, conventional indicators (e.g. chloride diffusivity and bulk electrical resistivity) recommended to assess corrosion rates of steel in PC cannot reliably reflect the corrosion behaviour in AAS.

3) The corrosion rate of the steel bars in the AAS concretes was significantly influenced by the free sulphide and $Na^+$ concentration. The influence of pore solution on corrosion needs to be studied in greater detail and a larger database of experimental results is required to accurately assess the electrochemical behaviour of the steel reinforcement in AAS.

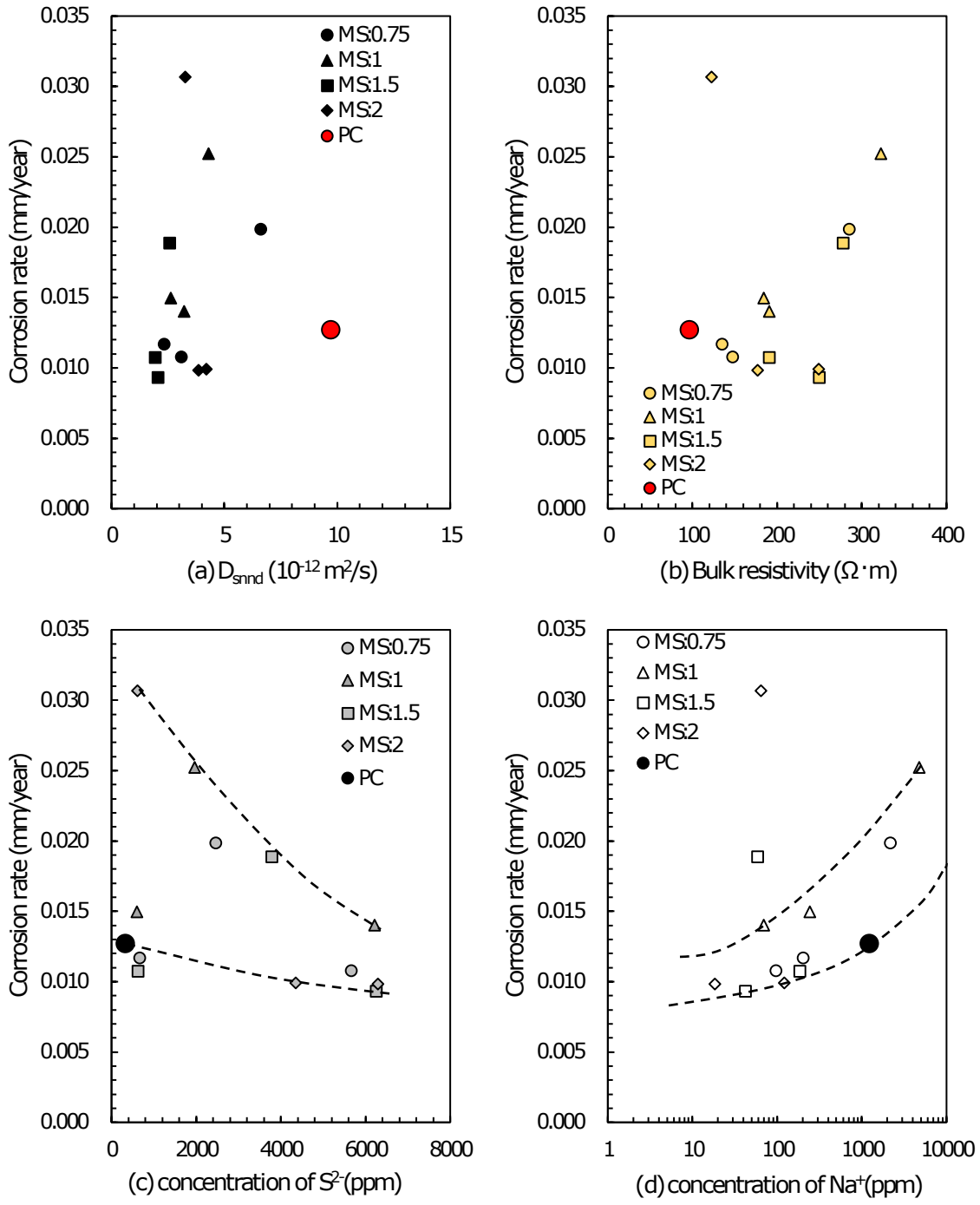


Figure 5 Correlations between corrosion rates and different contributing factors

**Acknowledgement**

The experiments described in this paper were carried out in the concrete laboratory of Queen's University Belfast and the authors acknowledge Queen's University for providing facilities for the investigation reported in this paper. The supports from University of Sheffield, Kunming University of Science and Technology and University of Leeds are highly appreciated as well. The authors thank financial supports provided by EPSRC (UK), NSFC (China) and the Open Research Funds for the Shenzhen University (China) and State Key Laboratory of High Performance Civil Engineering Materials (China).

**References**

1. Shi C, Krivenko PV, Roy D (2006) Alkali-activated cements and concretes. Taylor & Francis, London.
2. Puertas F, Fernandez-Jimenez A, Blanco-Varela MT (2004) Pore solution in alkali-activated slag cement pastes. Relation to the composition and structure of calcium silicate hydrate. Cement Concrete Research 34:139–148
3. Criado M, Bernal SA, Garcia-Trinanes P, Provis JL (2018) Influence of slag composition on the stability of steel in alkali-activated cementitious materials. Journal of Materials Science 53(7): 5016-5035
4. Ismail I, Bernal SA, Provis JL, San Nicolas R, Brice DG, Kilcullen AR, Hamdan S, van Deventer JSJ (2013) Influence of fly ash on the water and chloride permeability of alkali-activated slag mortars and concretes. Construction Building Materials 48: 1187–1201
5. Provis JL, Myers RJ, White CE, Rose V, van Deventer JSJ (2012) X-ray microtomography shows pore structure and tortuosity in alkali-activated binders. Cement Concrete Research 42: 855–864
6. Ma QM, Nanukuttan S, Basheer PAM, Bai Y, Yang CH (2016) Chloride transport and the resulting corrosion of steel bars in alkali activated slag concretes. Materials and Structures 49: 3663-3677
7. Holloway M, Sykes JM (2005) Studies of the corrosion of mild steel in alkali-activated slag cement mortars with sodium chloride admixtures by a galvanostatic pulse method. Corrosion Science 47(12):3097–3110
8. BS EN 15167-1 (2006) Ground granulated blast furnace slag for use in concrete, mortar and grout—Part 1 Definitions, specifications and conformity criteria
9. BS EN 197-1 (2000) Cement—Part 1: Composition, specifications and conformity criteria for common cements
10. Yang C, Pu X (1993) Retarder of alkali activated slag, Chinese patent, 91108316.2
11. BS 1881-125 (1986) Testing concrete —Part 125: Methods for mixing and sampling fresh concrete in the laboratory
12. BS EN 12350-2 (2009) Testing fresh concrete Part 2: Slump-test
13. BS EN 12350-3 (2009) Testing hardened concrete Part 3: Compressive strength of test specimens
14. NT BUILD 443 (1995) Concrete, hardened: accelerated chloride penetration
15. NT BUILD 492 (1999) Concrete, mortar and cement-based repair materials: chloride migration coefficient from nonsteady-state migration experiments
16. Tang L (2005) Guideline for practical use of methods for testing the resistance of concrete to chloride ingress, Chlortest Report
17. Allahverdi A, Shaverdi B, Najafi KE (2010) Influence of sodium oxide on properties of fresh and hardened paste of alkali-activated blast-furnace slag. International Journal of Civil Engineering 8(4):304–314
18. Karahan O, Yakupoglu A (2011) Resistance of alkali-activated slag mortar to abrasion and fire. Advance Cement Research 23(6):289–297
19. Krizan D, Zivanovic B (2002) Effects of dosage and modulus of water glass on early hydration of alkali-slag cements. Cement Concrete Research 32(8):1181–1188
20. Al-Otaibi S (2008) Durability of concrete incorporating GGBS activated by water-glass. Constr Build Mater 22(10):2059–2067

21. Basheer PAM, Gilleece PRV, Long AE, Mc Carter WJ (2002) Monitoring electrical resistance of concretes containing alternative cementitious materials to assess their resistance to chloride penetration. Cement Concrete Composites 24(5):437–449
22. Whittington HW, McCarter J, Forde MC (1981) The conduction of electricity through concrete. Magazine Concrete Research 33(114):48–60
23. Tritthart J (1989) Chloride binding in cement II. The influence of the hydroxide concentration in the pore solution of hardened cement paste on chloride binding. Cement Concrete Research 19:683–691